

Renal cell carcinoma associated with Xp11.2 translocation/TFE gene fusion: imaging findings in 21 patients

Xiao Chen¹ · Qingqiang Zhu² · Baoxin Li³ · Wenjing Cui^{1,4} · Hao Zhou¹ · Na Duan¹ · Yongkang Liu¹ · Vikas Kundra⁵ · Zhongqiu Wang¹

Received: 18 August 2015 / Revised: 29 February 2016 / Accepted: 19 May 2016 / Published online: 2 June 2016
© European Society of Radiology 2016

Abstract

Objectives To characterize imaging features of renal cell carcinoma (RCC) associated with Xp11.2 translocation/TFE gene fusion.

Methods Twenty-one patients with Xp11.2/TFE RCC were retrospectively evaluated. Tumour location, size, density, cystic or solid appearance, calcification, capsule sign, enhancement pattern and metastases were assessed.

Results Fourteen women and seven men were identified with 12 being 25 years old or younger. Tumours were solitary and cystic-solid (76.2 %) masses with a capsule (76.2 %); 90.5 % were located in the medulla. Calcifications and lymph node metastases were each observed in 24 %. On unenhanced CT, tumour attenuation was greater than in normal renal parenchyma (85.7 %). Tumour enhancement was less than in normal renal cortex on all enhanced phases, greater than in normal renal medulla on cortical and medullary phases, but less than in normal renal medulla on delayed phase. On MR, the tumours were isointense on T1WI, heterogeneously

hypointense on T2WI and slightly hyperintense on diffusion-weighted imaging.

Conclusion Xp11.2/TFE RCC usually occurs in young women. It is a cystic-solid, hyperdense mass with a capsule. It arises from the renal medulla with enhancement less than in the cortex but greater than in the medulla in all phases except the delayed phase, when it is lower than in the medulla.

Key Points

- Xp11.2/TFE RCC was more prevalent in young women.
- On unenhanced CT, Xp11.2/TFE RCC attenuation was greater than in renal parenchyma.
- Xp11.2/TFE RCC arises primarily from the renal medulla.
- Xp11.2/TFE RCC enhancement was less than in the cortex on all phases.
- Enhancement was greater than in the medulla in arterial and corticomedullary phase.

Keywords Renal cell carcinoma · Xp11.2 translocation · TFE gene fusion · Multidetector computed tomography · Magnetic resonance imaging

Xiao Chen and Qingqiang Zhu contributed equally to this work.

✉ Zhongqiu Wang
zhq2001us@163.com

¹ Department of Radiology, Affiliated Hospital of Nanjing University of Chinese Medicine, 155 Hanzhong Road, Nanjing 210029, China

² Department of Medical Imaging, Subei People's Hospital, Medical School of Yangzhou University, No. 98 West Nantong Road, Yangzhou 225001, China

³ Department of Radiology, Gulou Hospital, Nanjing 210008, China

⁴ Department of Radiology, Jinling Hospital, Nanjing University Medical School, 305 east zhongshan Road, Nanjing 210002, China

⁵ Department of Radiology, The University of Texas, M.D. Anderson Cancer Center, 1515 Holcombe Boulevard, Houston, TX, USA

Abbreviations

RCC Renal cell carcinoma
CT Computed tomography
MR Magnetic resonance
ROI Region of interest

Introduction

The recently identified group of Xp11.2 translocation/TFE gene fusion renal cell carcinomas (Xp11.2/TFE RCC) affect approximately 15 % of patients under 45 years old with renal cell carcinoma [1]. Xp11.2/TFE RCC affects primarily

children and adolescents, and more commonly women [2–4]. Argani et al. reported that this tumour accounts for approximately 0.5 % of adult renal cell carcinoma, but 20 % of RCCs in young people [5]. According to the World Health Organization (WHO) classification of renal tumours, Xp11.2/TFE RCC is a distinct entity with unique pathologic/morphogenetic characteristics and biological behaviour [6, 7]. It has been associated with prior exposure to cytotoxic chemotherapy in childhood [8, 9]. Symptoms may include backache, abdominal pain, abdominal mass, haematuria and anaemia, but patients are commonly asymptomatic and the tumour is incidentally found. Pathologically, Xp11.2/TFE RCC originates from the renal medulla, which is different from the typical clear cell RCC that arises from the renal cortex.

Although Xp11.2/TFE RCCs have been reported from pathologic and clinical perspectives, there are only a few previous reports focusing on their radiological imaging findings. Recently, serial studies with small sample sizes (5–12 patients) described imaging findings of Xp11.2/TFE RCC [10–14]. Two larger sample size CT studies of Xp11.2/TFE RCC including 19 patients and 20 patients were reported by Woo et al. [15] and He et al. [16], respectively. CT and MR imaging features need further clarification/validation. In this study, we retrospectively investigated CT and MRI findings of 21 cases of Xp11.2/TFE RCC. Our purpose was to characterize the imaging features of RCC associated with Xp11.2 translocation/TFE gene fusion.

Materials and methods

Patients

Upon searching the hospital pathology and PACS systems, we identified 21 patients with pathologically proven Xp11.2/TFE RCC from the following three hospitals: Affiliated Hospital of Nanjing University of Chinese Medicine, Subei People's Hospital and Nanjing Jinling Hospital. Age, sex, tumour size, right or left location, surgery or biopsy finding, metastasis location and clinical symptoms were recorded. Patients with missing clinical or imaging data for review were excluded. This multicentre retrospective study was approved by the institutional review board with waiver of informed consent.

CT and MR imaging technique

Twenty-one patients had CT examinations and three patients also had an MR imaging. All exams were performed on one of several MDCT scanners (Somatom Definition, Siemens AG, Medical Solutions, Forchheim, Germany; Brilliance 64, Philips Medical Systems, Netherlands; Light Speed VCT, GE healthcare, USA). An abdominal unenhanced CT and

contrast-enhanced CT scan were performed on 21 patients. Parameters included detector collimation of 64×0.5 – 0.625 mm, gantry rotation time of 0.4–0.5 s, tube voltage of 120 kVp, abdominal reference tube current of 160–250 mAs and a field of view 35–40 cm. All images were reconstructed from the contrast-enhanced MDCT scan with 0.75 mm slice thickness and 0.5–5 mm reconstruction increment. Contrast-enhanced CT scan was started by continuously injecting a bolus of 80–100 ml of iopromide (300 mg/ml, Schering, Germany) followed by 40 ml saline solution into an antecubital vein via an 18-gauge catheter (injection rate 5 ml/s). The enhanced CT scans were performed at 20 s corticomedullary phase ($n=21$), 65 s nephrographic phase ($n=21$) and 240 s excretory phase (delayed phase, $n=11$).

MR was performed using a 3.0-T scanner (Siemens, Magnetom Trio) on three patients. All sequences were acquired with anterior and posterior saturation bands. The transverse planes covered the entire area of the kidneys. Baseline fast low-angle shot (FLASH) T1-weighted and fast spin echo T2-weighted breath-hold scans were first obtained. Then, an additional precontrast turbo-FLASH T1-weighted scan and diffusion-weighted imaging (DWI) scan were acquired. After intravenous injection of 0.1 mmol/kg gadolinium (3.5 ml/s), axial and sagittal turbo-FLASH T1-weighted images were obtained.

Pathology examination

At surgery and gross evaluation, specimens were assessed for shape; cystic components; fibrous capsule; invasion into the renal calyx, pelvis or ureter; and invasion into the renal vein or inferior vena cava (IVC). Pathological specimens were observed by haematoxylin–eosin staining and immunohistochemical analysis, including for TFE3 nuclear staining, P504S, EMA and CD10 [17]. Two uropathologists with 5–10 years of experiences interpreted the specimens. Xp11 translocation RCC diagnosis was confirmed by immunohistochemistry using antibodies (Abcam, Cambridge, USA) against TFE3 (C-terminal part of transcription factor binding to IGHM enhancer 3). All renal tumours were confirmed to be Xp11.2/TFE RCC from samples obtained at surgery ($n=19$) or biopsy ($n=2$). Slides were evaluated for growth pattern (papillary focal glandular, or alveolar), cell shape, architecture and nuclear grade.

Imaging and statistical analysis

Two genitourinary radiologists analysed the images together, a process that resulted in a consensus interpretation. The imaging parameters included the tumour position, size, cystic components or necrosis, calcification, tumour attenuation on unenhanced CT scan, the degree of enhancement (Hounsfield units, HU) on different phases of the enhanced CT scan,

lymphadenopathy, perinephric stranding, hydronephrosis, presence or absence of a clear tumour boundary (capsule sign), vascular invasion, and metastasis. For MR images, T1WI and T2WI signal, enhancement pattern and DWI signal were assayed besides the imaging parameters mentioned above. Unenhanced tumour HU was classified as mildly high if greater than 10 HU and high greater than 20 HU compared to normal renal parenchyma. The tumour was classified as a solid or cystic mass depending on predominance. The tumour was divided into solid (without obvious necrotic or cystic areas), cystic-solid (with solid and cystic components) and cystic (greater than 75 % of cystic) tumour. The density of the tumour, normal renal cortex, and medulla were measured during all enhanced phases. However, intratumoral calcification and cystic components if present were avoided. For the tumour, the measured area (the region of interest, ROI) was the centre of the mass in order to avoid partial volume effects. The normal renal cortex and medulla were measured in uninvolved unilateral renal cortex and medulla. Ten-millimetre ROIs were measured three times for each phase and the mean value was used. The enhancement pattern of the tumour was classified as homogeneous or heterogeneous. The degree of enhancement was based on the dynamic CT using Hounsfield unit values of the tumour, renal cortex and medulla.

Statistical analyses used SPSS13.0 statistical software. Data are expressed as mean \pm sd, and count data are expressed as percentage. Values were compared by ANOVA. $P < 0.05$ was considered statistically significant.

Results

Clinical characteristics

Patient characteristics are shown in Table 1. Among the 21 cases of Xp11.2/TFE RCC, the mean age at diagnosis was 27 ± 13 years (range 7–65 years). Most of patients were less than 45 years old (90.4 %, 19/21). Twelve patients' age was less than 25 years old and one was more than 65 years old. Xp11.2/TFE RCC was more common in women (66.7 %, 14/21), and more tumours involved the right kidney (76.2 %, 16/21). Flank pain, haematuria and palpable mass were found in 11 (52.4 %), 8 (38.1 %) and 5 (23.8 %) out of 21 patients, respectively.

CT imaging findings

CT and MR imaging findings are shown in Table 2 and Figs. 1, 2, and 3. Mean tumour diameter was 5.5 ± 2.4 cm (range 2.1–10.9 cm). Seventeen lesions were oval and four were irregular in shape. Xp11.2/TFE RCC was located in the renal medulla (Figs. 1a–f, 2) in 19 cases (90.5 %). Unexpectedly, two cases (10 %) were located in the renal

Table 1 Clinical data of 21 patients

Variables	Number of subjects
Age (years)	27.0 \pm 13.0 (7–65)
>25	9 (42.9 %)
\leq 25	12 (57.1 %)
Gender	
Male	7 (33.3 %)
Female	14 (66.7 %)
Side	
Left	5 (23.8 %)
Right	16 (76.2 %)
Flank pain	
Yes	11 (52.4 %)
No	10 (47.6 %)
Haematuria	
Yes	8 (38.1 %)
No	13 (61.9 %)
Palpable mass	
Yes	5 (23.8 %)
No	16 (76.2 %)

cortex (Fig. 3). Five cases (23.8 %, 5/21) had retroperitoneal lymph node metastases, and two cases (9.5 %, 2/21) also had a liver metastasis. Hydronephrosis was not seen in any case. Clear boundaries defined as a capsule sign were found in 16 cases (76.2 %) on the delayed phase (Figs. 2e, f, 3d) and five (23.8 %, 5/21) had part of the tumour with a poorly defined margin.

A solid mass (Figs. 1a, f, 2 and 3) was found in four cases (19.0 %). Cystic-solid mass (Figs. 1b, c, e, 4) was found in 16 cases (76.2 %). Cystic mass was found in one case (4.8 %). It was homogeneous (Figs. 1a, f, 2 and 3) in 19.0 % (4/21) of the cases and heterogeneous with cystic or necrotic components (Figs. 1b–e, 4) in 81.0 % (17/21) (Table 2). Calcifications (Figs. 1c, d, 3a) were seen in five masses (23.8 %).

Increased attenuation was found in tumours on pre-intravenous contrast images in 18 cases (85.7 %, Fig. 1). The CT attenuation (HU) of Xp11.2/TFE RCC was statistically significantly greater than in normal renal cortex or normal renal medulla (49.6 ± 6.4 vs 34.0 ± 1.7 or 30.2 ± 2.1 , $P < 0.05$, respectively) (Table 2). On unenhanced CT, the attenuation of Xp11.2/TFE RCC was high (>20 HU) in eight cases (38.1 %) or mildly high (10–20 HU) in ten cases (47.6 %) compared to normal renal cortex.

Imaging findings on dynamic contrast-enhanced CT scan are shown in Fig. 4. Enhancement of Xp11.2/TFE RCC was less than in normal renal cortex ($P < 0.05$) and more than in the medulla ($P < 0.05$) on the cortical phase and medullary phase, and less than in the cortex or medulla ($P < 0.05$) on the delayed phase, respectively.

Table 2 CT imaging findings

Clinical data	Value
Size (cm)	5.5 ± 2.4 (2.1–10.9)
Mass location	
Renal medulla	19 (90.5 %)
Renal cortex	2 (9.5 %)
Shape	
Oval	17 (81.0 %)
Irregular	4 (19.0 %)
Solid and cystic pattern	
Solid	4 (19.0 %)
Solid and cystic	16 (76.2 %)
Cystic	1 (4.8 %)
Calcification	
Yes	5 (23.8 %)
No	16 (76.2 %)
Unenhanced CT density	
High attenuation ^a	18 (85.7 %)
Iso-, hypo attenuation	3 (14.3 %)
Tumour CT density (enhanced)	
Homogeneous	4 (19.0 %)
Heterogeneous	17 (81.0 %)
Capsule sign	
Yes	16 (76.2 %)
No	5 (23.8 %)
Lymph node metastasis	5 (23.8 %)
Distant Metastasis	2 (9.5 %)
Renal or inferior vena cava invasion	1 (4.8 %)

^a More than 10 Hounsfield units compared with normal renal parenchyma

MR imaging findings

Three cases also underwent MRI (Figs. 5 and 6). The Xp11.2/TFE RCC was isointense on T1-weighted imaging, heterogeneous (Fig. 5b) or hypointense (Fig. 6b) on T2-weighted imaging and enhanced heterogeneously on contrast-enhanced imaging (Figs. 5d, e, 6c). Relatively high signal intensity was seen on diffusion-weighted magnetic resonance imaging (Fig. 5c). Tumour thrombus in the renal vein (Fig. 5d, f) and lymph node metastases (Fig. 6d) also could be observed. Necrotic or cystic components were found in tumours.

Histopathology findings

Tumour cells were arranged in primarily papillary architecture ($n = 11$, 52.4 %) and/or nested pattern with focal glandular and alveolar patterns. The tumour cells were polygonal with voluminous eosinophilic cytoplasm and high grade nuclear features (Fig. 7a). Foci of calcifications could be occasionally observed (Fig. 7b) in six cases. Immunohistochemistry staining

demonstrated TFE3 nuclear staining in all cases, (++) in nine cases and (+++) in 12 cases (Fig. 7c).

Discussion

Xp11.2/TFE RCC is a rare RCC subtype characterized by a number of different translocations involving the Xp11.2 chromosome. Histologically, the most distinctive feature is a carcinoma with predominantly papillary architecture composed of cells with somewhat voluminous, clear or slightly eosinophilic cytoplasm. The tumour cells strongly express TFE3 in the nucleus [18–22]. Argani et al. consider presence of TFE3 protein a strong immune marker of Xp11.2/TFE RCC that has both high sensitivity (97.5 %) and specificity (99.6 %) [5]. Although Xp11.2/TFE RCC has been reported in pathology studies [5], imaging reports are scant, particularly in combination with histopathologic examination and MR examination, and have consisted mainly of case reports [10–14]. Our data showed that the lesion is located in the renal medulla, is hyperdense or mildly hyperdense on unenhanced CT, has a characteristic enhancement pattern on contrast-enhanced studies and has a clear boundary (capsule sign) on the delayed phase of contrast-enhanced CT. On MR, the tumours were isointense on T1-weighted images, heterogeneous or low signal on T2-weighted images, increased signal on DWI and enhanced. Two studies have also evaluated characteristics of CT enhancement primarily [15, 16]. However, calcification and lymph node metastasis were only found in 23.8 % of cases in our study, which is less than in previous studies [14, 15]. Recently, He et al. also found low levels of calcification (30 %) and lymph node metastasis (15 %) [16], consistent with our study.

Imaging and surgery results showed that small Xp11.2/TFE RCC masses were located in the renal medulla, but unexpectedly two tumours appeared to arise from the cortex. Thus, ancillary imaging features such as enhancement pattern and patient age need to be considered for correct diagnosis. Other RCC types may also involve the renal medulla, e.g. parts of clear cell carcinoma [23–25], collecting duct carcinoma [26, 27], transitional cell carcinoma [28], squamous cell carcinoma [29], papillary RCC and chromophobe RCC [30] and renal medullary carcinoma [31, 32]. It is difficult to differentiate Xp11.2/TFE RCC from other tumours if only relying on tumour location. Other characteristics can be helpful. For example, about 94 % of cortical clear cell RCCs, the most common subtype, exhibit an expansible appearance with exophytic growth that disrupts the reniform contour [33] and enhancement is often similar to the cortex. Collecting duct RCC usually has no capsule [34]. Transitional cell RCC originates in the urinary collecting system and may cause hydronephrosis [35]. Chromophobe RCC may have a spoke-like pattern in some cases [27]. Renal medullary carcinoma

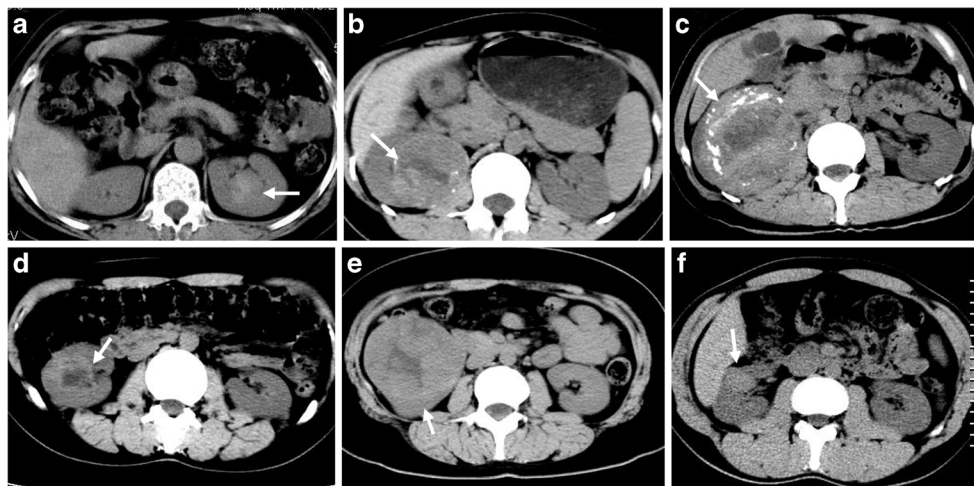


Fig. 1 Xp11.2/TFE RCC imaging findings on unenhanced CT images. a 2.0-cm-diameter slight hyperdense renal mass (50 HU) (arrow) compared with adjacent renal parenchyma (39 HU) in the left kidney of a 65-year-old woman. The mass is located in the renal medulla and impresses upon to the renal pelvis. b 6.0-cm-diameter slight hyperdense renal mass (52 HU) (arrow) located in the renal medulla in a 25-year-old woman. Calcification and cystic components were found in the mass. c An 8.4 cm-diameter hyperdense renal mass (58 HU) (arrow) in the medulla with calcifications in a 36-year-old woman. Mass density is

heterogeneous on unenhanced CT images and cystic components or necrosis can be found in the mass. d 3.9-cm-diameter heterogeneously hyperdense renal mass (46 HU) (arrow) located in the renal medulla in a 22-year-old woman. Cystic components or necrosis were found in the mass. e 8.6-cm-diameter slight hyperdense renal mass (34 HU) (arrow) compared with adjacent renal parenchyma (26 HU) located in the renal medulla in a 25-year-old woman. f 3.0-cm-diameter slight hyperdense renal mass (48 HU) (arrow) located in the renal medulla in a 26-year-old man. Mass density is homogeneous on unenhanced CT images

usually occurs in young people with sickle cell trait or disease [31], is hypovascular and shows an infiltrative pattern with ill-defined border [32]. Attention may also be paid to the attenuation on pre-intravenous contrast CT.

Our result showed that 86 % of Xp11.2/TFE RCCs are homogenous hyper- or mildly hyperattenuating solid tumours on unenhanced CT. Woo et al. reported that 68.4 % of masses were of high attenuation [15] on unenhanced CT. Other

authors reported that the pathologic basis of high density of a tumour on unenhanced CT was mainly due to intratumoral haemorrhage (haemosiderin deposition) [18]. The differential diagnosis of homogenous, slightly high or high attenuation solid renal mass on unenhanced CT can include clear cell RCC [23, 25], papillary RCC [24, 36], angiomyolipoma with minimal fat [37] and oncocytoma [38, 39]. On pre-intravenous contrast imaging, the Hounsfield units of clear cell, papillary

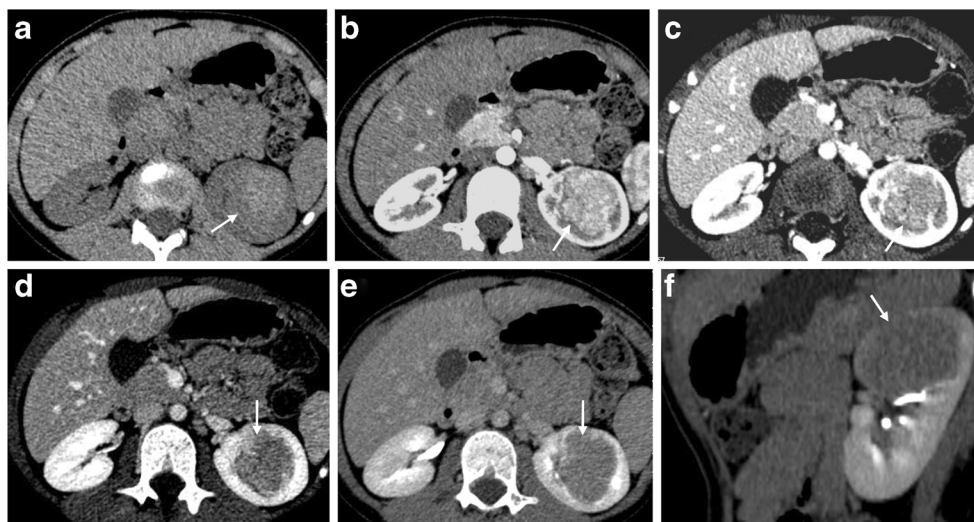
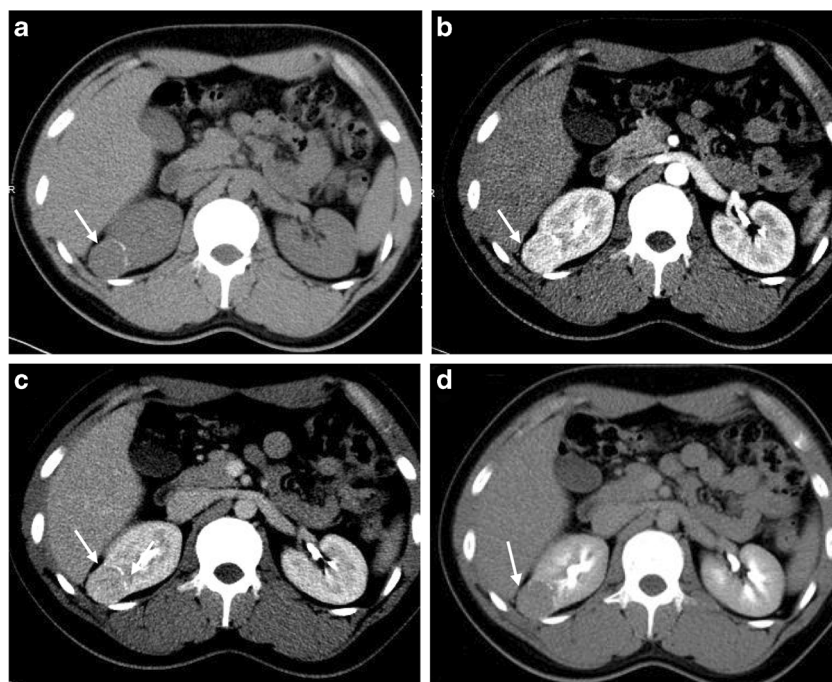


Fig. 2 Xp11.2/TFE RCC of left kidney in a 7-year-old girl. a Unenhanced CT scan showed a hyperdense mass (arrow) in the renal medulla; the density of the mass was 56 HU. b Homogeneous enhancement (145 HU) was noted during the corticomedullary phase (arrow). c During the nephrographic phase, the density of the tumour

increased to 164 HU (arrow). d Tumour density decreased to 120 HU during the early delayed phase, and a clear boundary was revealed (arrow). e Tumour density decreased to 106 HU during the delayed phase. f Coronal enhanced imaging on delayed phase shows the renal cortex involvement and pelvis displacement

Fig. 3 Xp11.2/TFE RCC of the left kidney in a 21-year-old man. a Unenhanced CT scan showed a hyperdense mass (arrow) in the renal cortex, the density of the mass was 42 HU. b

Homogeneous enhancement (120 HU) was noted during the corticomedullary phase (arrow). c During the nephrographic phase, the density of the tumour decreased to 118 HU (arrow). d Tumour density decreased to 86 HU during the delayed phase, and a clear boundary was revealed (arrow)



and chromophobe RCC average less than 40 HU [40]; whereas, it was 49 HU for Xp11.2/TFE RCC. Renal cell carcinomas larger than 3 cm often contain intratumoral necrosis, haemorrhage, cystic components and calcifications [23, 25] and they are usually of the clear cell variety [41]. Cystic-solid appearance was noted in 76.2 % of XP11.2/TFE RCCs in this study.

Two larger studies have evaluated characteristics of CT enhancement primarily [15, 16]. Woo et al. [15] evaluated tumour and cortex enhancement and found little difference

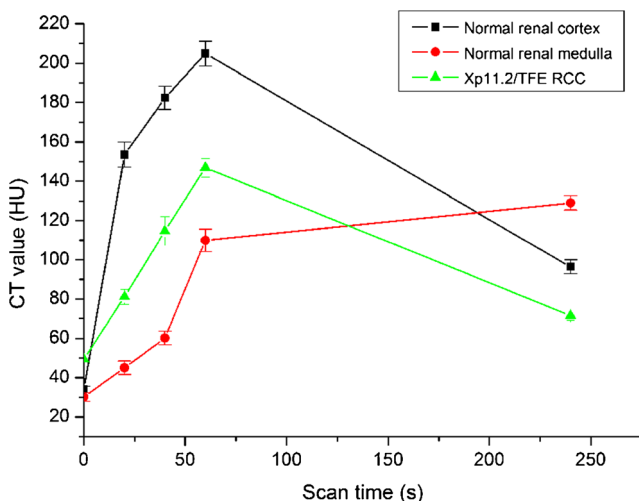


Fig. 4 Dynamic contrast-enhanced curve of XP11.2/TFE RCC. The CT values of tumours, normal renal cortex and renal medulla were 49.6 ± 6.4 , 34.0 ± 1.7 and 30.2 ± 2.1 Hounsfield units on unenhanced CT images, respectively. XP11.2/TFE RCC enhancement was less than in normal renal cortex ($n=21$) and more than in the medulla ($n=21$) on the corticomedullary phase and on the nephrographic phase, and less than in the cortex or medulla ($n=11$) on the delayed phase

in tumour enhancement between the cortical (30–40 s) and early delayed phases, but less enhancement than the cortex on both phases. He et al. [16] suggest less enhancement than the cortex on corticomedullary, nephrographic and early delayed phases (180 s), but similar enhancement to medulla on corticomedullary and less than medulla on nephrographic and early delayed phases. In this study, we also showed the dynamic contrast-enhanced features of Xp11.2/TFE RCC. In comparison, we found statistically significant fewer enhancements than cortex on corticomedullary phase, nephrographic phases and delayed phases, but increased attenuation compared to medulla on corticomedullary phases and less attenuation compared to medulla on delayed phase. The differences in enhancement pattern may be related to timing and patient population. Our study reports statistically significant differences to support our findings in enhancement patterns.

Like XP11.2/TFE RCC, some tumours are hypointense compared to the renal cortex on enhanced CT and MR imaging [23–25, 34, 36, 38, 42], e.g. papillary RCC, collecting duct RCC, chromophobe RCC, oncocytoma and renal lymphoma. The majority of papillary RCC show slight enhancement on all enhanced scan phases [24, 36], which is distinction from XP11.2/TFE RCC. Kato et al. considered the imaging findings of papillary RCC to be similar to Xp11.2/TFE RCC [18]. However, papillary RCC may be multifocal and bilateral, tends to be less than 2 cm in size at diagnosis [41], hypovascular and homogeneous [43]. Recently, Woo et al. [15] compared imaging findings of Xp11.2/TFE RCC with papillary RCC and suggested that larger size, more cystic change or necrosis, presence of calcification and high density on unenhanced CT imaging may be helpful for differentiating

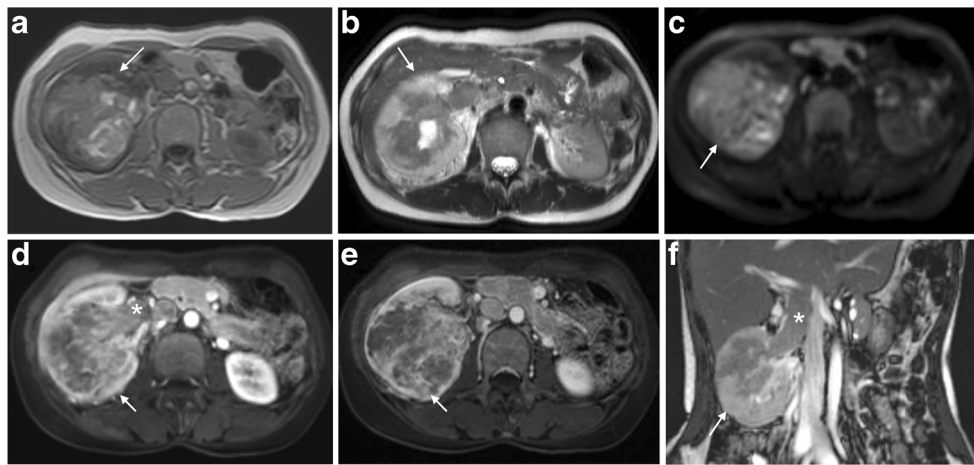


Fig. 5 MR imaging findings of Xp11.2/TFE RCC in a 46-year-old woman. a T1-weighted MR imaging revealed a 7.8-cm-diameter heterogeneously isointense right renal mass (arrow) with areas of hyperintensity compared to normal renal tissue. b T2-weighted MRI shows a mass (arrow) with heterogeneous increased intensity. c Relatively high signal intensity (arrow) was seen on diffusion-weighted magnetic resonance imaging ($b = 800$). d T1-weighted intravenous

contrast-enhanced MR imaging in the corticomedullary phase revealed a mass (arrow) with heterogeneous enhancement relative to that of the renal parenchyma. Tumour thrombus was observed in right renal vein (star). e T1-weighted delayed phase revealed that the mass (arrow) had heterogeneously less enhancement relative to the renal cortex. f Coronal delayed phase showed that the mass (arrow) had fewer enhancements relative to that of the renal cortex. Tumour thrombus was observed in renal vein (star)

XP11.2/TFE RCC from papillary RCC. We found a male to female ratio of 1:2, greater than 2:3 found by Woo et al. [15], and we found that the tumour epicentre is almost exclusively in the medulla (90.5 %). The presence of calcification and high attention (23.8 %) in our study was very close to that in papillary RCC (23.1 %) in a previous study [15] and thus may

not be a good distinguishing characteristic. In comparison, the degree of enhancement of XP11.2/TFE RCC can be higher than that of collecting duct RCC.

Kato et al. described of Xp11.2/TFE RCC on T2-weighted signal intensity as hypointense, [18]. In our MR case, slightly hypointense signal or heterogeneous signal on T2-weighted

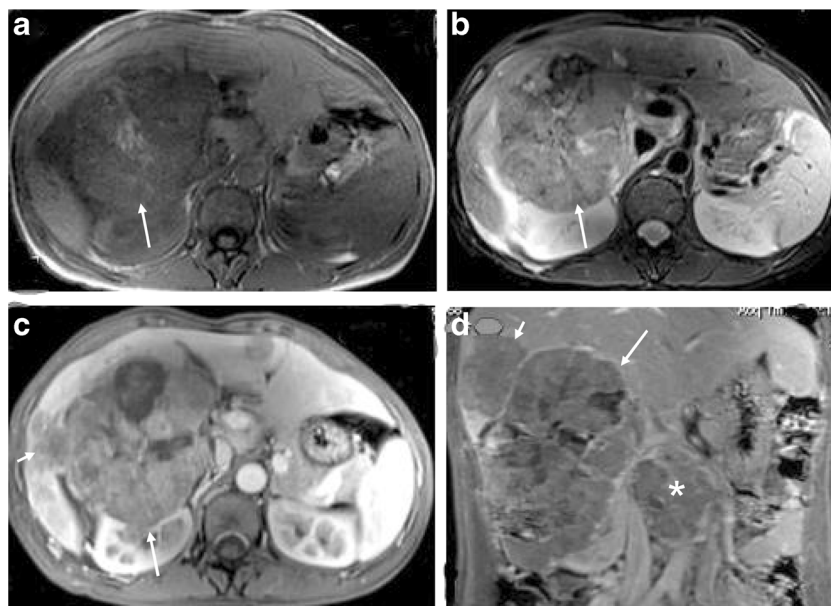


Fig. 6 MR imaging findings of Xp11.2/TFE RCC in a 30-year-old woman. a T1-weighted MR imaging revealed a heterogeneously isointense right renal mass with areas of hyperintensity. b Transverse T2-weighted MRI shows a mass (arrow) slightly hypointense relative to the renal parenchyma. c Transverse T1-weighted enhanced MR imaging on nephrographic phase revealed a mass (long arrow) with less

enhancement relative to the renal cortex. The hepatic metastasis (short arrow) was also seen. d Coronal T1-weighted enhanced MR imaging on delayed phase showed a heterogeneous mass with mild enhancement (arrow). The hepatic metastasis lesion (short arrow) and retroperitoneal lymph node metastasis (star) were also seen

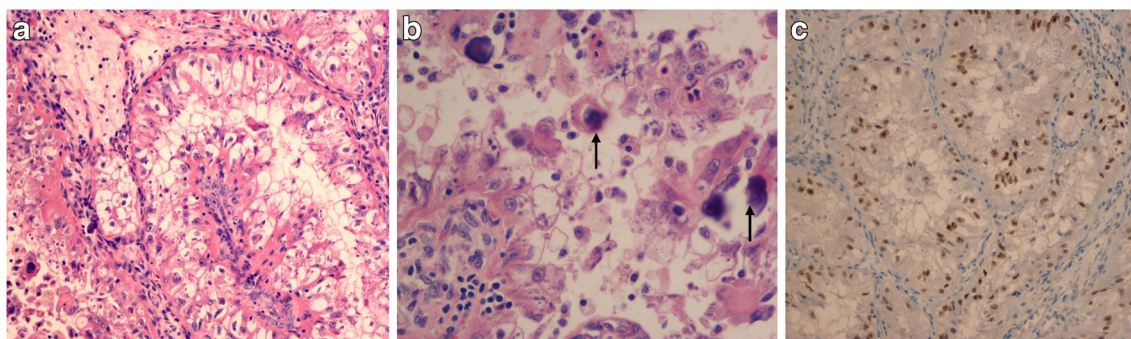


Fig. 7 Haematoxylin–eosin staining (a, b) and immunohistochemical (IHC) staining (c) for TFE3 protein in representative renal carcinoma with Xp11.2 translocations. a The tumour has a primarily papillary growth pattern (H&E stain; original magnification, $\times 100$). b Foci of

calcifications (arrows) were observed in tumour samples ($\times 200$). c Immunohistochemistry showed diffuse, strong TFE3 (+++) staining, SP method ($\times 100$)

imaging were observed. This is in distinction to many renal tumours that are hyperintense on T2-weighted imaging, such as clear cell RCC, some cystic renal tumours, and cysts. Larger clear cell RCCs tend to have a heterogeneous, hyperintense signal on T2-weighted MR imaging, separating them from Xp11.2/TFE RCC. Other renal tumours that may be hypointense on T2-weighted MR imaging include papillary RCC, lymphoma, chromophobe RCC and oncocytoma [37].

Eighteen cases had obvious complete or near complete boundaries on CT and MR imaging (capsule sign), which was best seen on delayed phase. This is consistent with the Xp11.2/TFE RCC capsule seen by pathology, and noted by previous studies [20, 44]. This may be a distinguishing feature from tumours without a clear boundary such as collecting duct RCC, poorly differentiated clear cell RCC, poorly differentiated papillary RCC and an inflammatory renal mass. In this study, we also found that Xp11.2/TFE RCC is more prevalent in young women. Moreover, 57 % of patients are less than 25 years old. Our data is consistent with some previous studies [14, 16]. However, Woo et al. showed that the mean age of patients with Xp11.2/TFE RCC is about 40 years old [15]. The differences may be related to patient population.

In routine clinical work, the rate of correct diagnosis of Xp11.2/TFE RCC by imaging is low. This is likely due to both a low incidence and a low level of awareness. A constellation of imaging features can help identify this subset. The prognosis of RCC is related to the histopathological subtypes [45]. Thus, the imaging features of Xp11.2/TFE RCC may be valuable for predicting the prognosis of RCC. In addition, it has been shown that the incidence of Xp11.2/TFE RCC may be underestimated because TFE3 nuclear staining is not performed during routine pathological examination [46]. Knowing the imaging features of Xp11.2/TFE RCC is helpful for improving pathological examination.

The main limitation to our study is that the number of patients with Xp11.2/TFE RCC is small; however, the number of cases of Xp11.2/TFE RCC in our study is bigger than any other series in the radiologic literature. Second, as a

multicentre study, there were mild differences in scanning parameters among the institutions. In addition, only three patients underwent MR examinations. The MR features of Xp11.2/TFE RCC need further investigation.

In conclusion, Xp11.2/TFE RCC is usually located in the renal medulla, hyper- or mildly hyperdense on unenhanced CT, heterogeneously hypointense on T2-weighted MR imaging and slightly hyperintense on DWI; moreover, it is less enhancing than the cortex on all phases, and more enhancing than the medulla on all phases except delayed, where it is less enhancing than the medulla. In addition, Xp11.2/TFE RCC usually has clear boundaries (capsule sign) with low frequency of calcifications and lymph node metastases. With such findings, Xp11.2/TFE RCC should be considered, particularly in young and middle-aged women.

Acknowledgments The scientific guarantor of this publication is Zhongqiu Wang. The authors of this manuscript declare no relationships with any companies whose products or services may be related to the subject matter of the article. This study is funded by the Priority Academic Program Development of Jiangsu Higher Education Institutions. No complex statistical methods were necessary for this paper. Institutional review board approval was obtained. Written informed consent was waived by the institutional review board. Some study subjects or cohorts have been previously reported in *Acta Radiologica*. Methodology: retrospective, multicentre study.

References

1. Komai Y, Fujiwara M, Fujii Y et al (2009) Adult Xp11 translocation renal cell carcinoma diagnosed by cytogenetics and immunohistochemistry. *Clin Cancer Res* 15:1170–1176
2. Meyer PN, Clark JI, Flanigan RC, Picken MM (2007) Xp11.2 translocation renal cell carcinoma with very aggressive course in five adults. *Am J Clin Pathol* 128:70–79
3. Parikh J, Coleman T, Messias N, Brown J (2009) Temsirolimus in the treatment of renal cell carcinoma associated with Xp11.2 translocation/TFE gene fusion proteins: a case report and review of literature. *Rare Tumors* 1:e53

4. Winarti NW, Argani P, De Marzo AM, Hicks J, Mulyadi K (2008) Pediatric renal cell carcinoma associated with Xp11.2 translocation/TFE3 gene fusion. *Int J Surg Pathol* 16:66–72
5. Argani P, Lal P, Hutchinson B, Lui MY, Reuter VE, Ladanyi M (2003) Aberrant nuclear immunoreactivity for TFE3 in neoplasms with TFE3 gene fusions: a sensitive and specific immunohistochemical assay. *Am J Surg Pathol* 27:750–761
6. Skolarus TA, Serrano MF, Berger DA et al (2008) The distribution of histological subtypes of renal tumors by decade of life using the 2004 WHO classification. *J Urol* 179:439–443, discussion 43–44
7. Lopez-Beltran A, Scarpelli M, Montironi R, Kirkali Z (2006) 2004 WHO classification of the renal tumors of the adults. *Eur Urol* 49:798–805
8. Argani P, Laé M, Ballard ET et al (2006) Translocation carcinomas of the kidney after chemotherapy in childhood. *J Clin Oncol* 24:1529–1534
9. Ramphal R, Pappo A, Zielenska M, Grant R, Ngan B-Y (2006) Pediatric renal cell carcinoma clinical, pathologic, and molecular abnormalities associated with the members of the mit transcription factor family. *Am J Clin Pathol* 126:349–364
10. Dang TT, Ziv E, Weinstein S, Meng MV, Wang Z, Coakley FV (2012) Computed tomography and magnetic resonance imaging of adult renal cell carcinoma associated with Xp11.2 translocation. *J Comput Assist Tomogr* 36:669–674
11. Koo HJ, Choi HJ, Kim MH, Cho KS (2013) Radiologic-pathologic correlation of renal cell carcinoma associated with Xp11.2 translocation. *Acta Radiol* 54:827–834
12. Liu K, Xie P, Peng W, Zhou Z (2014) Renal carcinomas associated with Xp11.2 translocations/TFE3 gene fusions: findings on MRI and computed tomography imaging. *J Magn Reson Imaging* 40:440–447
13. Zhu QQ, Wang ZQ, Zhu WR et al (2013) The multislice CT findings of renal carcinoma associated with Xp11.2 translocation/TFE3 gene fusion and collecting duct carcinoma. *Acta Radiol* 54:355–362
14. Wang W, Ding J, Li Y, Wang C, Zhou L, Zhu H, Peng W (2014) Magnetic resonance imaging and computed tomography characteristics of renal cell carcinoma associated with Xp11.2 translocation/TFE3 gene fusion. *PLoS One* 9:e99990
15. Woo S, Kim SY, Lee MS et al (2015) MDCT findings of renal cell carcinoma associated with Xp11.2 translocation and TFE3 gene fusion and papillary renal cell carcinoma. *AJR Am J Roentgenol* 204:542–549
16. He J, Gan W, Liu S, Zhou K, Zhang G, Guo H, Zhu B (2015) Dynamic computed tomographic features of adult renal cell carcinoma associated with Xp11.2 translocation/TFE3 gene fusions: comparison with clear cell renal cell carcinoma. *J Comput Assist Tomogr*. doi:10.1097/RCT.0000000000000263
17. Malouf G, Camparo P, Oudard S et al (2010) Targeted agents in metastatic Xp11 translocation/TFE3 gene fusion renal cell carcinoma (RCC): a report from the Juvenile RCC network. *Ann Oncol* 21:1834–1838
18. Kato H, Kanematsu M, Yokoi S et al (2011) Renal cell carcinoma associated with Xp11.2 translocation/TFE3 gene fusion: radiological findings mimicking papillary subtype. *J Magn Reson Imaging* 33:217–220
19. Argani P, Aulmann S, Karanjawala Z, Fraser RB, Ladanyi M, Rodriguez MM (2010) Xp11 translocation renal cell carcinoma (RCC): extended immunohistochemical profile emphasizing novel RCC markers. *Am J Surg Pathol* 34:1295–1303
20. Ross H, Argani P (2010) Xp11 translocation renal cell carcinoma. *Pathology* 42:369–373
21. Armah HB, Parwani AV (2010) Xp11.2 translocation renal cell carcinoma. *Arch Pathol Lab Med* 134:124–129
22. Argani P, Aulmann S, Karanjawala Z et al (2009) Melanotic Xp11 translocation renal cancers: a distinctive neoplasm with overlapping features of PEComa, carcinoma, and melanoma. *Am J Surg Pathol* 33:609–619
23. Sauk SC, Hsu MS, Margolis DJ et al (2011) Clear cell renal cell carcinoma: multiphasic multidetector CT imaging features help predict genetic karyotypes. *Radiology* 261:854–862
24. Ruppert-Kohlmayr AJ, Uggowitz M, Meissnitzer T, Ruppert G (2004) Differentiation of renal clear cell carcinoma and renal papillary carcinoma using quantitative CT enhancement parameters. *AJR Am J Roentgenol* 183:1387–1391
25. Soyer P, Dufresne A, Klein I, Barbagelatta M, Herve JM, Scherrer A (1997) Renal cell carcinoma of clear type: correlation of CT features with tumor size, architectural patterns, and pathologic staging. *Eur Radiol* 7:224–229
26. Albadine R, Schultz L, Illei P et al (2010) PAX8 (+)/p63(-) immunostaining pattern in renal collecting duct carcinoma (CDC): a useful immunoprofile in the differential diagnosis of CDC versus urothelial carcinoma of upper urinary tract. *Am J Surg Pathol* 34:965–969
27. Gong Y, Sun X, Haines GK, Pins MR (2003) Renal cell carcinoma, chromophobe type, with collecting duct carcinoma and sarcomatoid components. *Arch Pathol Lab Med* 127:e38–e40
28. Urban BA, Buckley J, Soyer P, Scherrer A, Fishman EK (1997) CT appearance of transitional cell carcinoma of the renal pelvis: Part 2. Advanced-stage disease. *AJR Am J Roentgenol* 169:163–168
29. Imbriaco M, Iodice D, Erra P et al (2011) Squamous cell carcinoma within a horseshoe kidney with associated renal stones detected by computed tomography and magnetic resonance imaging. *Urology* 78:54–55
30. Kondo T, Nakazawa H, Sakai F et al (2004) Spoke-wheel-like enhancement as an important imaging finding of chromophobe cell renal carcinoma: a retrospective analysis on computed tomography and magnetic resonance imaging studies. *Int J Urol* 11:817–824
31. Davis CJ Jr, Mostofi FK, Sesterhenn IA (1995) Renal medullary carcinoma. The seventh sickle cell nephropathy. *Am J Surg Pathol* 19:1–11
32. Blitman NM, Berkenblit RG, Rozenblit AM, Levin TL (2005) Renal medullary carcinoma: CT and MRI features. *AJR Am J Roentgenol* 185:268–272
33. Zagoria RJ, Wolfman NT, Karstaedt N, Hinn GC, Dyer RB, Chen YM (1990) CT features of renal cell carcinoma with emphasis on relation to tumor size. *Investig Radiol* 25:261–266
34. Yoon SK, Nam KJ, Rha SH et al (2006) Collecting duct carcinoma of the kidney: CT and pathologic correlation. *Eur J Radiol* 57:453–460
35. Vikram R, Sandler CM, Ng CS (2009) Imaging and staging of transitional cell carcinoma: part 2, upper urinary tract. *AJR Am J Roentgenol* 192:1488–1493
36. Tsuda K, Kinouchi T, Tanikawa G et al (2005) Imaging characteristics of papillary renal cell carcinoma by computed tomography scan and magnetic resonance imaging. *Int J Urol* 12:795–800
37. Lee-Felker SA, Felker ER, Tan N, Margolis DJ, Young JR, Sayre J et al (2014) Qualitative and quantitative MDCT features for differentiating clear cell renal cell carcinoma from other solid renal cortical masses. *AJR Am J Roentgenol* 203:W516–W524
38. Gakis G, Kramer U, Schilling D, Kruck S, Stenzl A, Schlemmer HP (2011) Small renal oncocytomas: differentiation with multiphase CT. *Eur J Radiol* 80:274–278
39. Honda H, Bonsib S, Barloon TJ, Masuda K (1992) Unusual renal oncocytomas: pathologic and CT correlations. *Urol Radiol* 14:148–154
40. Zhang J, Lefkowitz RA, Ishill NM et al (2007) Solid renal cortical tumors: differentiation with CT. *Radiology* 244:494–504
41. Frank I, Blute ML, Cheville JC, Lohse CM, Weaver AL, Zincke H (2003) Solid renal tumors: an analysis of pathological features related to tumor size. *J Urol* 170:2217–2220

42. El-Sharkawy MS, Siddiqui N, Aleem A, Diab AA (2007) Renal involvement in lymphoma: prevalence and various patterns of involvement on abdominal CT. *Int Urol Nephrol* 39:929–933
43. Roy C, Sauer B, Lindner V, Lang H, Saussine C, Jacqmin D (2007) MR imaging of papillary renal neoplasms: potential application for characterization of small renal masses. *Eur Radiol* 17:193–200
44. Jayasinghe C, Siegler N, Leuschner I, Fleischhack G, Born M, Muller AM (2010) Renal cell carcinoma with Xp11.2 translocation in a 7-year-old boy. *Klin Padiatr* 222:187–189
45. Gudbjartsson T, Hardarson S, Petursdottir V, Thoroddsen A, Magnusson J, Einarsson GV (2005) Histological subtyping and nuclear grading of renal cell carcinoma and their implications for survival: a retrospective nation-wide study of 629 patients. *Eur Urol* 48:593–600
46. Komai Y, Fujiwara M, Fujii Y, Mukai H, Yonese J, Kawakami S et al (2009) Adult Xp11 translocation renal cell carcinoma diagnosed by cytogenetics and immunohistochemistry. *Clin Cancer Res* 15:1170–1176